ELSEVIER

Coordination Chemistry Reviews
216–217 (2001) 55–63

COORDINATION CHEMISTRY REVIEWS

www.elsevier.com/locate/ccr

Dinuclear metal complexes and ligands: stabilities and catalytic effects

Arthur E. Martell *, Jiri Perutka, Deyuan Kong

Department of Chemistry, Texas A&M University, College Station, TX 77842-3012, USA

Received 8 August 2000; received in revised form 15 November 2000; accepted 17 November 2000

Contents

Abstract

Two new dinucleating macrocyclic ligands, **1** and **2**, were designed and synthesized in our laboratory. Two phenolate donor groups were built into the macrocycles to increase the binding affinity for Fe(III). The stabilities of the iron(III) complexes of **1** and **2** are shown. These ligands were also found to complex iron(II) in the same manner, with the two Fe(II) ions bridged by the two phenolate oxygens. The stability constants of the Fe(II) chelates of **1** and **2** are also shown. The Fe(II) complexes were found to catalyze the oxidation of hydrocarbons, such as adamantane, by molecular oxygen.

Keywords: Dinucleating macrocyclic ligand; Fe(II) complex; Fe(III) complex; Oxidation; Adamantane; Stability constants

* Corresponding author. Tel.: +1-979-8455055; fax: +1-979-8454719.
E-mail address: martell@mail.chem.tamu.edu (A.E. Martell).

0010-8545/01/$ - see front matter
PII: S0010-8545(00)00407-0

1. Stability of mononuclear and dinuclear iron(III) and iron(II) complexes of 1 and 2

When two (or more) OH^- occur as bridging species, they are written as the equivalent O^{2-} (μ-oxo) species. Actually, the potentiometric method cannot distinguish between $2OH^-$ (μ-hydroxo) and O^{2-} (μ-oxo).

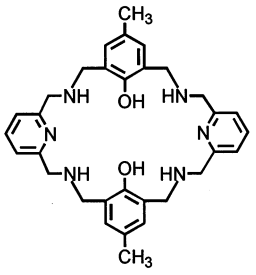

1

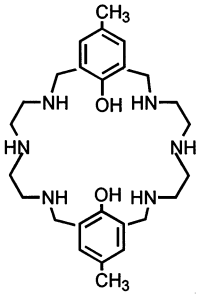

2

1.1. Fe(III) complexes of *1*

The overall and stepwise stability constants for the ligand (**1**)–Fe(III) system are included in Table 1 [1,2]. Three mononuclear and five dinuclear complexes were identified with very high stability constants.

The species distribution diagram of the system H_6L^{4+}–$2Fe^{III}$ are shown in Fig. 1 [1,2]. It is seen that the mononuclear $[Fe^{III}H_2L]^{3+}$ complex predominates from pH 2 to 3. Then the other ferric ion coordinates to the macrocycle to form the dinuclear ferric complex $[Fe_2^{III}L]^{4+}$ and reaches a maximum concentration (27%) at pH 3.1. Between pH 3.5 and 7, the μ-hydroxo bridged diferric complex $[Fe_2^{III}$(μ-

Table 1
Logarithms of stability constants of Fe(III) complexes of **1** [a]

Stoichiometry					
L	Fe^{3+}	H	Log β	Stepwise quotient	Log K
1	1	0	32.02	[FeL]/[Fe][L]	32.02
1	1	1	41.08	[LFeH]/[LFe][H]	9.06
1	1	2	47.99	$[LFeH_2]$/[LFeH][H]	6.91
1	2	0	44.99	$[Fe_2L]$/[FeL][Fe]	12.89
1	2	−1	41.99	$[Fe_2L]/[Fe_2L(OH)][H]$	2.92
1	2	−2	34.65	$[Fe_2L(OH)]/[Fe_2L(OH)_2][H]$	7.38
1	2	−3	25.64	$[Fe_2L(OH)_2]/[Fe_2L(OH)_3][H]$	9.01
1	2	−4	15.37	$[Fe_2L(OH)_3]/[Fe_2L(OH)_4][H]$	10.27

[a] **1** = H_2L.

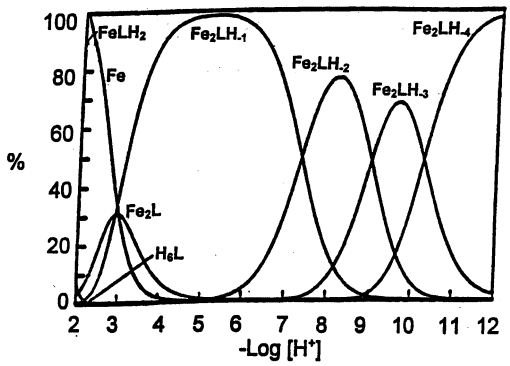

Fig. 1. Species distribution diagram for the L–Fe(III) system as a function of p[H] ($H_2L = 1$, $Fe = Fe^{3+}$, $T_{Fe(II)} = 2T_L = 4.00 \times 10^{-3}$ M). Only major species are shown: LFeH, LFe and $LFeH_{-1}$ (1%) which are minor species are omitted.

$OH)L]^{3+}$ dominates. Above $pH > 7$, the μ-oxo bridged diferric complex $[Fe_2^{III}(\mu\text{-}O)L]^{2+}$ and its further hydrolytic species become the main components in aqueous solution.

1.2. Fe(II) complexes of **1**

pH titration curves were employed to calculate 1:1 and 1:2 ligand (**1**):metal binding constants, together with constants involving protonated, deprotonated, and hydroxo-bridged species shown in Table 2 [1]. Four mononuclear and three dinuclear complexes were identified with fairly high stability constants for the ferrous ion-ligand system. The species distribution diagram of the system $H_6L^{4+} - 2Fe^{II}$ is shown in Fig. 2. When $pH < 5$, the ligand exists as various protonated species in solution. Between pH 5 and 7, the mononuclear ferrous complex forms and reaches the maximum concentration (72%) at pH 5.7. The conversion of the 1:1

Table 2
Logarithms of stability constants of Fe(II) complexes of **1** [a]

Stoichiometry					
L	Fe^{2+}	H	Log β	Stepwise quotient	Log K
1	1	0	15.32	[FeL]/[Fe][L]	15.32
1	1	1	26.0	[LFeH]/[LFe][H]	10.68
1	1	2	35.24	$[LFeH_2]/[LFeH][H]$	9.24
1	1	3	40.10	$[LFeH_3]/[LFeH_2][H]$	4.86
1	2	0	25.20	$[Fe_2L]/[FeL][Fe]$	9.88
1	2	1	31.22	$[Fe_2LH]/[Fe_2L][H]$	6.02
1	2	−1	15.29	$[Fe_2L]/[Fe_2L(OH)][H]$	9.91

[a] **1** = H_2L.

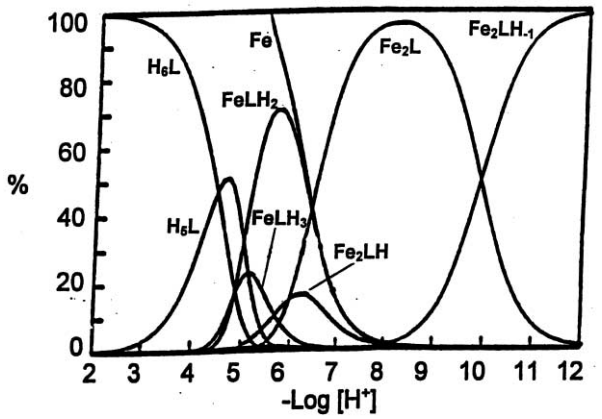

Fig. 2. Species distribution diagram for the L–Fe(II) system as a function of p[H] ($H_2L = 1$, $Fe = Fe^{2+}$, $T_{Fe(II)} = 2T_L = 4.00 \times 10^{-3}$ M). Only major species are shown: LH_4 and LFe_2H_2 (1%) are omitted.

into 1:2 complexes occurs about pH > 7, when a second ferrous ion enters the same macrocycle to form dinuclear ferrous complexes (maximum concentration 94% at pH 8.1). Finally, the hydroxo-bridged species $[Fe^{II}_2(\mu\text{-}OH)L]^{1+}$ dominates when pH > 10.

*1.3. Fe(III) complexes of **2***

The overall and stepwise stability constants for the ligand–Fe^{III} system for **2** are listed in Table 3 [4]. The data in Table 3 show that the addition of a second metal ion $[Fe^{III}L]^{+}$ to form $[Fe^{III}_2L]^{4+}$ is characterized by a lower stability constant than that of $[Fe^{III}L]^{+}$, because of the destabilization resulting from the coulombic

Table 3
Logarithms of stability constants of Fe(III) complexes of **2** [a]

Stoichiometry					
L	Fe^{3+}	H	Log β	Stepwise quotient	Log K
1	1	0	31.77	[FeL]/[Fe][L]	31.77
1	1	1	42.02	[FeHL]/[FeL][H]	10.25
1	1	2	48.65	$[FeH_2L]/[FeH][H]$	6.63
1	2	0	42.24	$[Fe_2L]/[FeL][Fe]$	15.42
1	2	−1	39.06	$[Fe_2(OH)L]/[Fe_2L][H]$	−3.18
1	2	−2	34.01	$[Fe_2(OH)_2L][H]/[Fe_2(OH)L]1$	−5.05
1	2	−3	24.27	$[Fe_2(OH)_3L[H]]/[Fe_2(OH)_2L]$	−9.75
1	2	−4	14.23	$[Fe_2(OH)_4L][H]/[Fe_2(OH)_3L]$	−10.03

[a] **2** = H_2L.

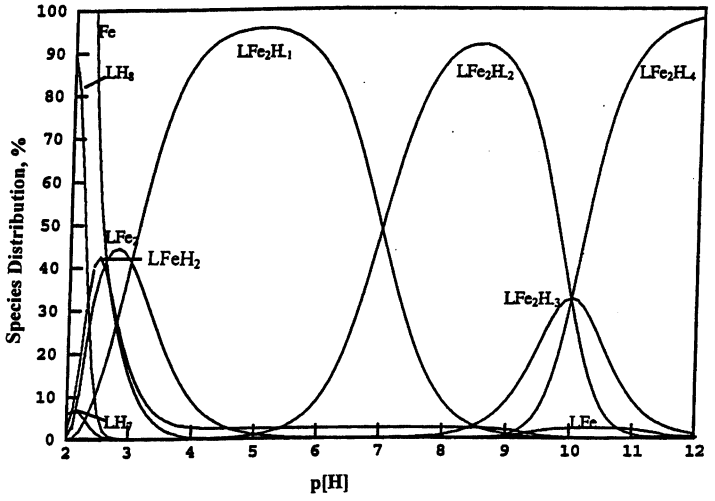

Fig. 3. Species distribution diagram for the L–2Fe(III) system as a function of p[H] ($H_2L = 2$, $Fe = Fe^{3+}$) (% = percentage of species distribution in solution).

repulsion between the two metal ions in the limited macrocyclic cavity. Wang et al. [1] also reported this trend in similar work on Fe(III). Three mononuclear and five dinuclear complexes were identified with high stability constants. The formation constant of the dinuclear complex of **1** is log K $[Fe_2^{III}L]^{3+} = 12.89$, compared with L log K $[Fe_2^{III}L]^{3+} = 15.42$, is lower by 2.54 logarithm units. This means the flexible groups in **2** are more suitable for the formation and high stability of dinuclear iron complexes.

The species distribution diagram of the system H_8L–$2Fe^{III}$ for **2** is shown in Fig. 3 [3]. It is seen that the mononuclear $[Fe^{III}H_2L]^{3+}$ complex predominates from p[H] 2 to 3. Then the other ferric ion enters into the macrocyclic cavity to form the dinuclear ferric complex $[Fe_2^{III}L]^{4+}$ and reaches a maximum concentration (44%) at pH 2.8. When the pH is raised, μ-hydroxo ferric complex $\{Fe_2(OH)L]^{3+}$ forms and reaches a maximum concentration 95.6% at pH 4.9. Between p[H] 4 and 7, the stable μ-hydroxo bridged diferric complex $[Fe_2^{III}(\mu\text{-}OH)L]^{3+}$ dominates. Above pH 7–10, the hydrolytic species $[Fe_2^{III}(\mu\text{-}O)L]^{2+}$, $[Fe_2^{III}(\mu\text{-}O)$, $(\mu\text{-}OH)L]^{+}$ and $[Fe_2^{III}(\mu\text{-}O)_2L]$ are formed successively. The μ-oxo bridged diferric complexes become the main components in aqueous solution at high pH.

*1.4. Fe(II) complexes of **2***

The stability constants involving protonated, deprotonated and hydroxo-bridged Fe(II) species of **2** are shown in Table 4 [3]. For mononuclear systems, three major species $[Fe^{II}H_4L]^{4+}$, $[Fe^{II}HL]^{+}$ and $[Fe^{II}L]$ were identified with high concentrations

of species and fairly high stability constants. The formation constant of log $K_{[FeL]}$ is 18.88 which is larger than that of **1** (log $K_{[FeL]} = 15.32$, Table 2).

The species distribution curves indicate that $[FeLH_2]$ begins to dominate when the pH is higher than 5.5, and reaches its highest concentration at pH 6 (90%). In the dinuclear system (Fig. 4), $[Fe_2L]^{2+}$ is formed and two hydroxo-bridged species: $[Fe_2(OH)L]^{3+}$ and $[Fe_2(OH)_2L]^{2+}$ dominate in the range pH 7–12 [3]. Dinuclear complexes easily form hydroxo-bridged hydrolytic species.

Table 4
Logarithms of stability constants of Fe(II) complexes of **2** [a]

Stoichiometry					
L	Fe^{2+}	H	Log β	Stepwise quotient	Log K
1	1	0	18.88	[FeL]/[Fe][L]	18.88
1	1	1	29.31	[FeHL]/[FeL][H]	10.43
1	1	2	37.60	$[FeH_2L]/[FeH][H]$	8.29
1	1	3	44.26	$[FeH_3L]/[FeH_2L][H]$	6.68
1	1	4	49.12	$[FeH_4L]/[FeH_3L][H]$	4.86
1	2	0	26.38	$[Fe_2L]/[FeL][Fe]$	7.50
1	2	1	18.34	$[Fe_2(OH)L][H]/[Fe_2L]$	−8.04
1	2	1	8.38	$[Fe_2(OH)_2L][H]/[Fe_2(OH)L]$	−9.96

[a] **2** = H_2L.

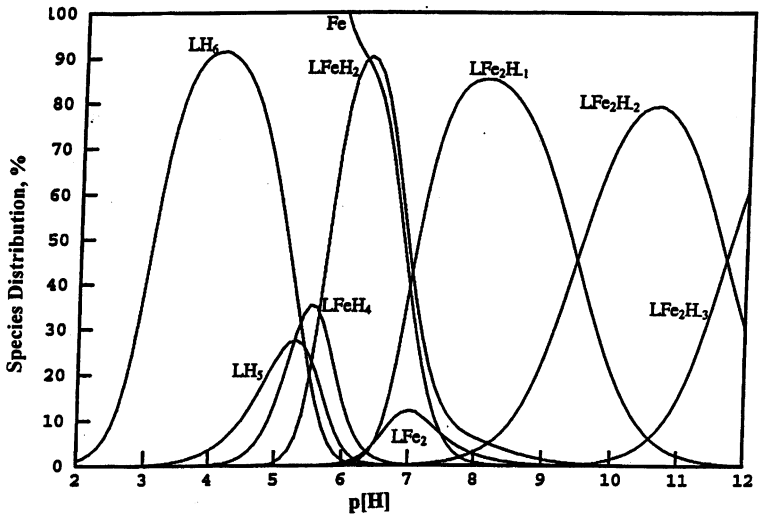

Fig. 4. Species distribution diagram for the L–2Fe(II) system as a function of p[H] ($H_2L = 2$, $Fe = Fe^{2+}$) (% = percentage of species distribution in solution).

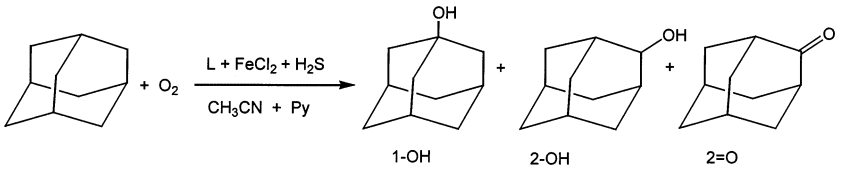

Scheme 1.

Table 5
Oxidation of adamantane by O_2 in the presence of H_2S with **1** as catalyst [a]

Solvent	Time (h)	1-OH (mmol)	2-OH (mmol)	2=O (mmol)	Turnover
CH_3CN	2	0.10	0.29	0	3.7
CH_3CN	4	0.87	0.75	0	15.2
CH_3CN	6	1.13	0.88	0	20.1
CH_3CN	8	1.27	1.05	0	23.0
CH_3CN	10	1.51	1.22	0	27.3
CH_3CN	20	2.38	2.13	0	45.1

[a] Catalysis by dinuclear Fe(II) complexes of **1**.

Table 6
Catalysis by dinuclear Fe(II) complexes of **2**

Solvent	Time (h)	1-OH (mmol)	2-OH (mmol)	2=O (mmol)	Turnover
CH_3CN	2	0.023	0.871	0.015	4.40
CH_3CN	4	0.30	0.93	0.020	5.69
CH_3CN	6	0.12	0.11	0.069	12.11
CH_3CN	8	0.14	0.14	0.078	14.18
CH_3COCH_3	1	0.032	0.071	0	4.10
CH_3COCH_3	4	0.047	0.11	0	6.12
CH_3COCH_3	6	0.064	0.15	0	8.74
CH_3COCH_3	8	0.11	0.24	0	14.00

2. Oxidation of adamantane

The overall oxidation reactions are shown in Scheme 1, which shows the organic substrate and reaction products. The results obtained for the hydroxylation of adamantane are summarized in Tables 5 and 6 [3,4].

It is interesting that the oxidation of adamantane produces only hydroxylation products (Table 5). The ratio of tertiary adamantanol to secondary adamantanol is around 1.2 for both catalysts. No ketonization product is observed even when the turnover is 45.1 after 20 h. A similar result was obtained by Kitajima [5], who reported only a trace of a ketonization product.

The effectiveness of the catalytic oxidation of adamantane is approximately at the same level as Kitajima's catalyts [5]. The dinuclear macrocyclic iron(II) complexes described are among the most effective functional models of methane monooxygenase reported thus far.

Compared with the **1**, **2** has a more flexible cavity and can accommodate the two iron ions at lower coulombic repulsions. The results obtained for the hydroxylation of adamantane are summarized in Table 6. The turnover numbers have been calculated as the following: turnovers = the sum of mmols of products/mmols of catalyst.

It is interesting that the oxidation of adamantane produces not only hydroxylation but also ketonization products, Wang et al. [1,2] and Kitajima [5] reported no or only a trace of ketonization products formed with different macrocyclic ligands as catalysts. When the solvent was changed to acetone, in similar conditions, no ketonization products were detected and the turnover was also somewhat lower. This observation is the same as observed for the GIF system [6]. The regioselectivity of 1-OH and 2-OH + 2-O varied with time. From 2 to 6 h, the selectivity of C2/C3 is nearly 3.6. When the reaction time was prolonged, the C2 products increase slowly compared with the C3 product (1-OH), and the ratio of C2/C3 was reduced to 1.5.

3. Procedure for oxidation reactions

A total of 15 ml of KOH (0.001 M) was added to 0.025 mmol of the macrocyclic ligand to neutralize the hydrogen bromide. The solution obtained was evaporated to dryness under vacuum. The light yellow oil was dissolved in 40 ml of CH_3CN, and then 0.05 mmol $FeCl_2{\cdot}4H_2O$ was added to initiate iron complex formation. After the mixture was stirred for 10 min at room temperature, the solution turned dark violet signifying the formation of the dinuclear iron complex $[Fe_2L]^{2+}$. While stirring was continued, 15 mmol adamantane was added, and then 1.0 ml pyridine was added. Hydrogen sulfide (2 ml min^{-1}) and dioxygen (20 ml min^{-1}) were simultaneously passed through the solution. After successive 1 or 2 h periods, 1 ml of the reaction mixture was filtered from the deposited sulfur and the solution was analyzed. The sample was quantitatively analyzed with a HP-5890 Series II gas chromatograph with solid naphthalene as an internal standard.

The oxidation of adamantane seem to be catalyzed by the macrocycles **1** and **2**, but the effect of pyridine has yet to be explored. This will be the subject of further investigation.

Acknowledgements

This research was supported by a grant from The Robert A. Welch Foundation (A-0259).

References

[1] Z. Wang, A.E. Martell, R.J. Motekaitis, J.H. Reibenspies, J Chem. Soc. Dalton Trans. (1999) 2441.
[2] J. Perutka, A.E. Martell, Anal. Chim. Acta (in press).
[3] D. Kong, A.E. Martell, R.J. Motekaitis, Ind. Eng. Chem. Res. 39 (2000) 3429.
[4] Z. Wang, A.E. Martell, R.J. Motekaitis, J.H. Reibenspies, Inorg. Chim. Acta 330-302 (2000) 378.
[5] (a) N. Kitajima, H. Fukui, Y. Moro-oka, J. Chem. Soc. Chem. Commun. (1988) 485. (b) N. Kitajima, M. Ito, H. Fukui, Y.J. Moro-oka, J. Chem. Soc. Chem. Commun. (1991) 102.
[6] D.H.R. Barton, W.D. Ollis, J.F. Stoddart, Comprehensive Organic Chemistry, vol. 1, Pergamon Press, Oxford, 1979, p. 108.